PHILOSOPHICAL TRANSACTIONS OF THE ROYAL SOCIETY A MATHEMATICAL, PHYSICAL & ENGINEERING SCIENCES

Chaos-Enhanced Transport in Cellular Flows

S. C. Jana and J. M. Ottino

Phil. Trans. R. Soc. Lond. A 1992 **338**, 519-532
doi: 10.1098/rsta.1992.0018

Chaos-enhanced transport in cellular flows

By S. C. Jana and J. M. Ottino

Department of Chemical Engineering, Northwestern University, Evanston, Illinois 60208, U.S.A.

Examples of chaos-enhanced transport in cellular flows are presented. Illustrations span from boundary and jet-induced motions within cavities to separated flows; chaotic advection is generated by time-modulation of walls, variation of angle of impingement of laminar jets, and naturally occurring oscillations in the velocity field as the Reynolds number is increased. Tools include manifold structure, the Melnikov technique, as well as eulerian and lagrangian descriptions of transport. A range of Péclet numbers is explored; the amount of transport enhancement over the non-chaotic case is exemplified in terms of heating of a fluid and the removal of a diffusive tracer; the enhancement over the non-chaotic case can be as large as 40%.

1. Introduction

Flow and transport in the vicinity of indentations, wedges and cavities, separated flows near corners, bluff bodies and steps, are all-too-common in technology and nature. Transport is hindered by wall-anchored streamlines, closed streamlines (cells), or arrays of cells of ever diminishing strength, as in the celebrated Moffatt's flow (Moffatt 1964); we term such flows cellular flows. Little is known on how to improve transport in such flows. Consider, for example, the case of wet cleaning of wafers for microelectronic applications (Chilukuri & Middleman 1983, 1984; Tighe & Middleman 1985). The aim is to remove residual contaminants contained in cavities within the surface of the wafer by flushing the surface with a cleaning fluid; however, according to the aspect ratio of the cavities there might be closed cells. Typical cavity sizes might range from thousands of microns for rough materials to tenths of microns for polished wafers; the typical Reynolds numbers range from 10^{-3} to 10^{4}. Timescales for diffusion – for a molecular diffusion coefficient of the order of 10^{-5} cm^2 s^{-1} – range from 10^{-5} to 10^{3} s and, for Reynolds numbers in the range 10–10^{4}, the rate of removal is controlled by molecular diffusion, which is typically slow. Thus, one question that suggests itself is the determination of flow conditions which result in the elimination of stagnant fluid regions within cavities and lead to efficient removal of the impurities. One possibility that comes to mind is to generate chaotic advection to enhance transport but it is unclear whether or not chaos can actually penetrate deep into the cavity. This is one of the questions addressed in this paper; the goal is to present an array of possibilities to motivate further work and to indicate the series of steps necessary for the analysis of related systems.

Several aspects of cellular flows, especially flows in cavities and wedges, have received considerable attention in the literature (Moffatt 1964; Pan & Acrivos 1967; Jeffrey & Sherwood 1980; Küblbeck *et al.* 1980; Chien *et al.* 1986; Chebbi & Tavoularis 1990). By contrast studies focusing on *transport enhancement* by means of

Phil. Trans. R. Soc. Lond. A (1992) **338**, 519–532
Printed in Great Britain

chaos in flows of practical interest are relatively recent and more scarce. The closest related studies have been carried out primarily in the context of the Rayleigh–Bénard (RB) flow (Solomon & Gollub 1988; Camassa & Wiggins 1990) and the Taylor–Couette (TC) flow (Broomhead & Ryrie 1988), both flows leading to spatially periodic arrays of cells. Experimental work in the RB flow has been carried out by Solomon & Gollub (1988) and recent theoretical work has been conducted by Camassa & Wiggins (1990). These studies show that time-periodic flows cause chaotic advection and improve inter-cell transport. Both the TC and the RB flows lead to spatially periodic cell structures with equal strengths and transport enhancement is predominantly in the direction parallel to the walls. By contrast the flows considered here are spatially non-periodic, neighbouring cells have widely different strengths, and the central issue is transport away from non-slip walls.

The analysis of chaotic advection starts with the analysis of the velocity field; in turn, chaotic advection forms a template for the evolution of transport. The most tractable cases correspond to Stokes and transitional two-dimensional flows and, fortunately, many processes of practical interest, such as the cleaning problem alluded to earlier, fall in this range. The simplest case to analyse corresponds to analytically determined velocity fields (see, for example, Chaiken *et al.* 1986; Swanson & Ottino 1990). However, in most cases of practical interest analytical solutions are not available and the problems must be solved numerically, for example, using finite-difference or boundary integral methods. Finite-difference techniques are, in principle, applicable for any Reynolds number and are particularly effective in regular geometries. Boundary integral methods, on the other hand, are well suited for Stokes flow problems involving complicated geometries.

Two prototypical flows are considered in some detail: closed cavity flows with moving walls and jet-induced flow in a cavity; a third flow, an oscillatory flow in a backward step is discussed only in qualitative terms. The paper is organized as follows: §2 describes the flows of interest, §3 gives a brief review of dynamical systems and topology of two-dimensional flows along with a discussion of possible mechanisms for generation of chaotic advection; §4 presents a brief analysis of the chaotic template (i.e. assuming that the tracers are purely passive); and §5 addresses the effect of chaos on the transport of diffusive tracers. Finally, §6 presents a discussion of the results and outlines a range of future problems and possibilities.

2. Flows of interest

The simplest class of flows we consider are closed-cavity Stokes flows generated by means of two walls sliding parallel to themselves (figure 1). Both co-rotating and counter-rotating wall motions lead to an array of elliptic points, the number of which depends on the aspect ratio (w = width/height) and the instantaneous ratio of the velocities of the walls ($r = U_{\text{top}}/U_{\text{bot}}$). However, only co-rotating wall motions (i.e. both walls move in opposite directions) lead to hyperbolic fixed points (Leong 1990). Here we restrict our attention to cavities leading to two counter-rotating cells (both walls move in the same direction); this situation leads to wall anchored dividing streamlines. Velocity fields can be obtained analytically (Weiss-Florsheim 1965) as well as numerically (Burggraf 1966; Pan & Acrivos 1967; Ryu *et al.* 1986). We use the approximate analytical solution by Weiss & Florsheim (1965) as the topology of the steady flows and the location of the elliptic and hyperbolic fixed points derived from this solution agree reasonably well with experiments (Leong 1990; see figure 1).

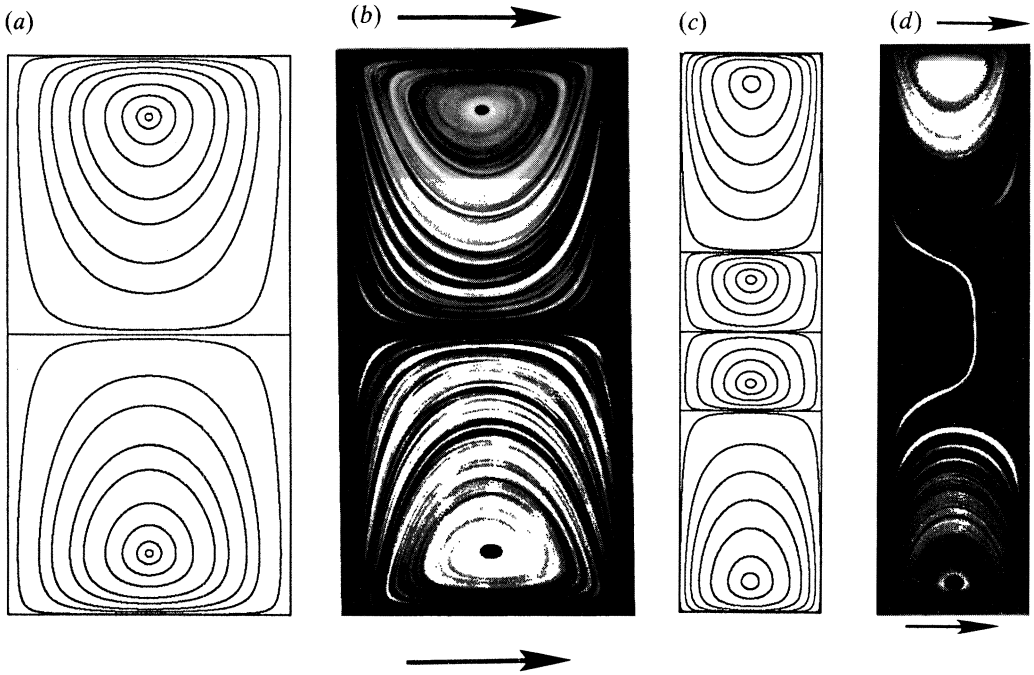

Figure 1. Steady streamline portraits for flow in a driven rectangular cavity. (*a*) Computation with $r = 1$ and $w = 0.5$. (*b*) Experiment with $r = 1$ and $w = 0.5$. (*c*) Computation with $r = 1$ and $w = 0.25$. (*d*) Experiment with $r = 1$ and $w = 0.25$. Both the top and bottom walls move from left to right.

The second type of flow – analysed by means of boundary integral technique (Higdon 1985, 1990) – is produced by impinging a laminar jet at the fluid trapped inside a rectangular cavity with depth H and aspect ratio w (figure 2). The free-stream velocity field is given by $u = axy + by^2$, $v = (-\frac{1}{2})ay^2$, with a jet angle $\alpha = \arctan(3a/2b)$. In this particular instance only part of the fluid from the cavity is washed away by the jet and the remaining fluid forms recirculating regions; the area of the recirculating region(s) and the number of cells depend on w and α. The third example, considered only briefly here as an example of a flow that becomes time-periodic as the Reynolds number is increased, is the flow down a backward step with height h (figure 3). A 'primary' separation bubble is formed at the step, which grows with increasing Reynolds number; at some critical Reynolds number the velocity field becomes time-periodic (further information about locations, number and sizes of bubbles, as well as the range of Reynolds numbers for which the flow is laminar, transitional, or turbulent can be found in the work by Armaly *et al.* (1983)). The height of the closed cavity, the depth of the open cavity, and the height of the backward step are taken to be equal to unity.

The starting point in the analysis is the streamline portrait and it is convenient to make a few comments in this regard. Typically, the determination of the streamline portrait involves the contouring of the value of streamfunctions at grid points. However, such technique might not be useful unless the flow is solved directly in terms of the streamfunction. Another possibility is to plot the velocity vector at grid points. In general, however, it is more convenient to integrate the velocity field, $\mathrm{d}\boldsymbol{x}/\mathrm{d}t = \boldsymbol{v}(\boldsymbol{x})$, for a number of strategically located initial conditions $\boldsymbol{X}$. Highly accurate interpolation routines, such as bicubic splines, must be used to ensure

PHILOSOPHICAL TRANSACTIONS OF THE ROYAL SOCIETY A MATHEMATICAL, PHYSICAL & ENGINEERING SCIENCES

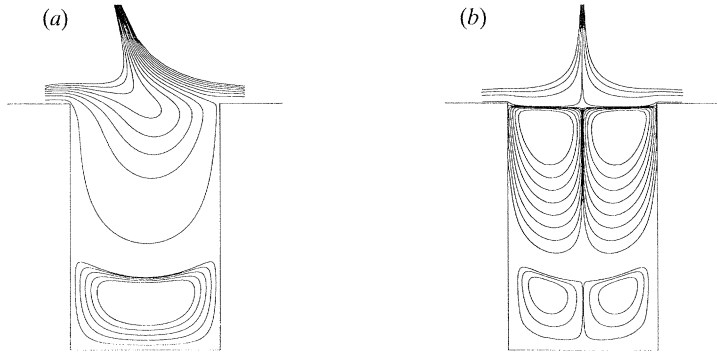

Figure 2. Steady streamline portraits for jet-induced flow in a rectangular cavity. (*a*) $\alpha = 75°$ and $w = 0.6$. (*b*) $\alpha = 90°$ and $w = 0.6$.

Figure 3. Steady streamline portrait for flow down a backward step. The Reynolds number is 250 and the channel length is 20. A parabolic laminar profile at the inlet and Dirichlet boundary condition at the outlet are used. The solution is obtained using the finite-difference code developed by Kim & Moin (1985).

streamline closure in the recirculating regions. Such a problem might arise, for example, in the flow down a backward step.

One important feature shared by all the flows considered here is dividing streamlines connecting two no-slip walls (heteroclinic streamlines). Figure 1*a*, *b* show the streamline portrait of a driven cavity flow with $w = 0.5$ and $r = 1$. In this case there are only two primary cells separated by a dividing streamline attached to the vertical walls. Figure 1*c*, *d* show streamline portrait for the same flow corresponding to a condition leading to four cells; the circulation in central cells is so weak – a factor of 10^3 with respect to the cells near the moving walls – that almost no deformation of a line of dye placed vertically across the cavity is observed in the timescale of the experiment. Figure 2 shows the streamline portrait corresponding to the jet-induced cavity flow for $\alpha = 75°$ and 90°. For $\alpha = 75°$ the cell structure is symmetric and occupies about 30% of the cavity. For $\alpha = 90°$ the topology of the flow is radically different; however, the position of the separating streamline remains virtually unchanged. Figure 3 shows the backward step flow corresponding to a Reynolds number $\rho U_{\max} h/\mu = 250$ ($U_{\max}$ is the maximum velocity of the entering parabolic profile, ρ and μ are the density and viscosity of the fluid respectively). At this Reynolds number the flow separates from the tip of the step and reattaches downstream at $7.685h$. All these flows can produce chaotic advection if the velocity field is made time-periodic. Let us, however, review a few dynamical systems concepts before venturing into chaotic advection and transport considerations (for a more complete exposition the reader is referred to Ottino (1989)).

3. Critical and periodic points: flow manipulation

The equations of motion for a two-dimensional area preserving velocity field can be written as

$$u = \mathrm{d}x/\mathrm{d}t = \partial\psi/\partial y, \quad v = \mathrm{d}y/\mathrm{d}t = -\partial\psi/\partial x, \tag{1}$$

PHILOSOPHICAL TRANSACTIONS OF THE ROYAL SOCIETY A MATHEMATICAL, PHYSICAL & ENGINEERING SCIENCES

PHILOSOPHICAL TRANSACTIONS OF THE ROYAL SOCIETY A MATHEMATICAL, PHYSICAL & ENGINEERING SCIENCES

Table 1. *Characteristics of* (*a*) *critical and* (*b*) *periodic points in two-dimensional time-periodic velocity fields*

(Critical points: solutions of $\boldsymbol{v}(\boldsymbol{P},t)=0$; eigenvalues of $D[\boldsymbol{v}(\boldsymbol{x},t)]$ at $\boldsymbol{P}$ determine the character. Periodic points: solutions of $\Phi_n(\boldsymbol{P})=\boldsymbol{P}$, $n=1,2,3,\ldots$; eigenvalues of $D[\Phi_n(\boldsymbol{P})]$ at $\boldsymbol{P}$ determine character.)

type	region of appearance	eigenvalues	local velocity or motion	difficulty in finding	contribution to chaos
(*a*)					
elliptic	fluid	$\lvert\lambda_i\rvert=1,\ i=1,2$	$u=Ky,\ v=-x$ $-1<K<0$	relatively easy	negative
hyperbolic	fluid: surfaces with slip	λs real; $\lambda_1<1<\lambda_2$	$u=Ky,\ v=x$ $0<K<1$	relatively easy	essential
parabolic	no-slip surface	$\lambda_{1,2}=\pm1$	with separation, $u=\alpha xy+\beta y^2,\ v=\gamma y^2$; without separation, $u=y,\ v=0$	easy with analytical $\boldsymbol{v}(\boldsymbol{x},t)$; difficult with numerical $\boldsymbol{v}(\boldsymbol{x},t)$	essential
(*b*)					
elliptic	fluid	$\lvert\lambda_i\rvert=1,\ i=1,2$	solid body rotation	lower orders easy if $\boldsymbol{v}(\boldsymbol{x},t)$ is analytical; otherwise difficult	negative
hyperbolic	fluid	λs real; $\lambda_1<1<\lambda_2$	stretching–contraction	lower orders easy if $\boldsymbol{v}(\boldsymbol{x},t)$ is analytical; otherwise difficult	essential
parabolic	fluid; slip-surface	$\lambda_{1,2}=\pm1$	shear	lower orders easy if $\boldsymbol{v}(\boldsymbol{x},t)$ is analytical: otherwise difficult	essential

Table 2. *Characteristics of various dynamical tools*

tool	Poincaré section	manifold structure	Melnikov method	stretching plots
characteristics	reduces dimensionality; reveals regular and chaotic regions and symmetry (if section time is appropriate); numerical	reveals regions of transport and high stretching; low period points provide the template of mixing; numerical	detects chaos; estimates lobe area; analytical if unperturbed homo/ heteroclinic orbits are analytical; in others cases semi-analytical	delineate the areas of high and low stretching
applicability	any perturbation	any perturbation	small perturbation	any perturbation
potential difficulties	none, if the velocity field is accurate; relatively robust under discretization	resolution is lost after few periods; computationally expensive	use somewhat limited for numerically obtained velocity field	computationally expensive; somewhat susceptible to error if numerical velocity field is used

where ψ is the streamfunction. If the velocity field is steady, i.e. ψ is independent of time, the velocity field is integrable and the system cannot be chaotic. On the other hand, if the velocity field, or equivalently ψ, is time-periodic there is a good chance that the system will be chaotic (Aref 1984). A necessary condition for chaos is that streamline portraits at two successive times show crossing of streamlines (recall that the *instantaneous* streamline portraits need not have any critical hyperbolic points in order for the flow to produce chaos).

The path of a fluid particle $\boldsymbol{x} = (x, y)$ initially located at $\boldsymbol{x}_0 = (x_0, y_0)$ corresponds to the solution of (1) with the initial condition $\boldsymbol{x} = \boldsymbol{x}_0$. The solution of (1) for all $\boldsymbol{x}_0$s belonging to the flow domain is called the *flow* or *motion* and is denoted as

$$\boldsymbol{x} = \boldsymbol{\Phi}_t(\boldsymbol{x}_0) \quad \text{with} \quad \boldsymbol{x}_0 = \boldsymbol{\Phi}_{t=0}(\boldsymbol{x}_0) \tag{2}$$

signifying that the fluid particle initially located at $\boldsymbol{x}_0$ will be found at position $\boldsymbol{x}$ at time t. In the case of time-periodic flows the flow can be reduced to a mapping. Given a flow $\boldsymbol{x} = \boldsymbol{\Phi}_t(\boldsymbol{x}_0)$, $\boldsymbol{P}$ is a *fixed point* of the flow if

$$\boldsymbol{P} = \boldsymbol{\Phi}_t(\boldsymbol{P}) \tag{3}$$

for all time t (i.e. the particle located at the position $\boldsymbol{P}$ stays at $\boldsymbol{P}$); equivalently $\boldsymbol{v}(\boldsymbol{P}, t) = \boldsymbol{0}$ for all t. Fixed or critical points corresponding to isochoric two-dimensional flows can be hyperbolic or saddle type, elliptic, or parabolic; the character of the fixed point can be obtained by linearizing the *velocity field* near $\boldsymbol{P}$. A companion concept is that of *periodic* points. At point $\boldsymbol{P}$ is periodic, of period nT, if

$$\boldsymbol{P} = \boldsymbol{\Phi}_{nT}(\boldsymbol{P}) \tag{4}$$

for $n = 1, 2, 3, \ldots$ but not for any $t < nT$ (fixed points are also periodic points but with zero period). Here n defines the *order* of the periodic point and T is the period of the flow. A common notation for $\boldsymbol{\Phi}_{nT}(\cdot)$ is $\boldsymbol{f}^n(\cdot)$. The character of the periodic point can be obtained by linearizing the *mapping* near $\boldsymbol{P}$. Periodic points can be hyperbolic, elliptic, or parabolic (see table 1). There is a subtle but important difference between periodic points and critical points. A periodic point is a material point; a critical point is not. Thus, if one were able to place a labelled fluid particle at any arbitrary time on a periodic point the particle will faithfully record the motion of the periodic point for all times. Such a thought experiment is not possible with a critical point and in particular it is not possible with a critical point corresponding to a separating streamline, which happens to be the primary point of interest in our case. In a no-slip boundary, fluid particles adhere to the wall; nevertheless the flow can be manipulated – for example by increasing the Reynolds number in the backward step problem – in such a way that the location of the attaching point; i.e. the location where vorticity changes sign can be changed at will. The same is true for flows manipulated by means of boundary motions. As an example, figure 4 shows the motion of point of separation (or reattachment) as a function of wall motions in the wall-driven cavity flow (see also figure 1*a*, *b*). Chaos is unlikely unless separation and attachment points do move; in this particular case the motion leads to the chaotic structure shown in figure 5*a*.

The dynamics of low-order periodic points plays a profound role in producing chaos. Elliptic points occur in the interior of islands that preclude mixing. Hyperbolic points occur within the fluid whereas parabolic points originated by flow separation occur at no-slip boundaries. Both types of points have associated

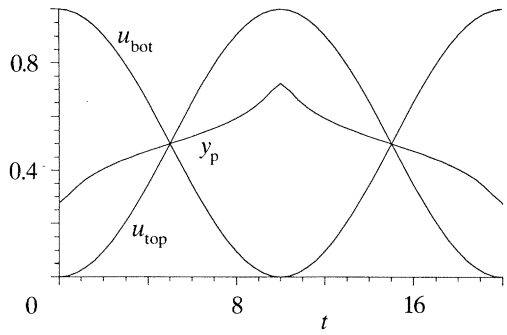

Figure 4. Location of the point of separation in a period in the driven cavity flow; $r = 1$, $w = 0.5$, and $T = 20$. The wave-form for the wall motion is given in equation 5.

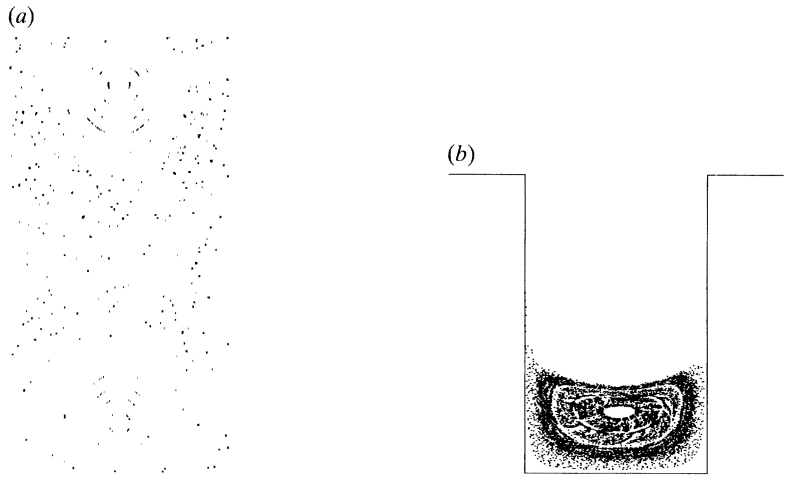

Figure 5. Poincaré sections for time-periodic flows. (*a*) Flow in a closed rectangular cavity. $r = 1$, $w = 0.5$, and $T = 20$, (*b*) flow in open cavity. $\alpha_1 = 75°$, $\alpha_2 = 90°$, $w = 0.5$, $T = 50$, $a = 1000$.

manifolds that constitute the primary avenues for transport. The local stable (unstable) manifold is the set of all points which tend to the fixed point as $t \to +\infty(-\infty)$. In our case the manifolds of interest are those associated with separation and reattachment points. If the flow is steady, stable and unstable manifolds join smoothly (as in figures 1–3) and transport is poor. To enhance transport the manifolds have to intersect transversely; this can occur if the flow is made time-periodic.

There are several ways to introduce a time-periodic perturbation. In the case of flows with inertia, such as the backward step flow, this occurs naturally as the Reynolds number is increased; related examples occur in Taylor–Couette flow (Davey *et al.* 1968; Mullin *et al.* 1987), driven cavity flows (O'Brien 1975; Goodrich & Soh 1989), and periodic vortex shedding behind a cylinder (Shariff *et al.* 1991). Stokes flows, on the other hand, have to be manipulated from 'outside' and there is no natural timescale. A common prescription is the time-periodic motion of the boundaries. Time-periodic motion of only one wall is not sufficient to produce chaos in a Stokes flow – the streamline portrait is invariant upon changes in direction and magnitude in the motion of a wall – and consequently at least two walls must be

moved (see Leong & Ottino 1989). The walls can be modulated in a number of ways, but only square and sine square wave-forms, with walls moving in the same direction, are used in this work. In the square wave, each wall is moved at a constant speed for half of a period. In the sine square wave, the top and bottom walls are moved according to:

$$u_{\text{top}} = U_{\text{top}} \sin^2(\pi t/T + \tfrac{1}{2}\pi), \quad u_{\text{bot}} = U_{\text{bot}} \sin^2(\pi t/T). \tag{5}$$

The advantage of the sine square wave over the square wave is that we can easily cast the perturbed dynamical system into the standard form for the Melnikov analysis presented in §4. To a large extent the results are independent of the details of the motion and depend only on the period (Swanson 1991).

Jet-induced cavity flows can be made chaotic by varying the angle of impingement in a time-periodic manner; the period is defined with respect to $1/aH\,(a \neq 0)$. The cellular structures formed at the bottom of the cavity for jet angles other than 90° are nearly symmetric. However, for 90° there is a change in the topology of the flow. Even though the jet does not penetrate completely into the cavity, it forces the fluid to split into recirculating regions, which appear in pairs with a line of symmetry around the y axis at half the width of the cavity (figure 2*b*). In this work we use jet angles of 75° and 90° and apply them alternately; this prescription leads to substantial streamline crossing. As we shall see however, the regions of chaos are separated by a wall anchored Kolmogorov–Arnold–Moser (KAM) surface – possibly leaky – that prevents the material at the bottom from being effectively removed by the flushing jet.

4. Underlying chaos

The effects of time-periodic perturbations on flows can be analysed using tools of dynamical systems theory. The main techniques are Poincaré sections, manifold structures, lobe dynamics, stretching plots, Melnikov method, etc. Table 2 gives a summary of the general features of these tools; only a few aspects of these techniques are exploited here.

Poincaré sections are used to determine the main structures in the flow; i.e. locations and extents of regular and chaotic regions. Figure 5*a* shows a typical Poincaré section for the closed-cavity flow; KAM surfaces separate the remnants of the regular regions from the chaotic regions (see figure 1*a*). Similarly figure 5*b* focuses on the bottom part of a jet-induced cavity flow. The motion in the bottom region is a factor of 10^{-3} weaker than the upper part of the flow and high period jets are needed to generate substantial chaos. Particles above the separation streamline leave the cavity under the action of the high-period jets.

It is important to stress that even if Poincaré sections show the existence of substantial communications between the different cellular regions, the rate of transport might in fact be very poor (see Khakhar *et al.* 1987, especially fig. 16). Other tools are necessary to investigate transport rate; this is done by studying the manifold structures of low-order periodic points, in particular the manifolds associated with the separating and attaching streamlines.

The analysis of these issues can proceed along the lines put forward by Wiggins *et al.* (see, for example, Rom-Kedar & Wiggins 1990), and it goes by the name of lobe dynamics. By determining the number and motion of lobes – the area trapped between successive primary intersections of stable and unstable manifolds – it is possible to compute the mass being transferred from one region to another per period

PHILOSOPHICAL TRANSACTIONS OF THE ROYAL SOCIETY A MATHEMATICAL, PHYSICAL & ENGINEERING SCIENCES

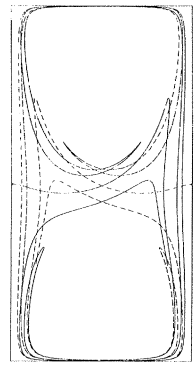

Figure 6. Manifold structures of closed cavity flow after 12 periods; $r = 1$, $w = 0.5$, and $D = 20$; continuous line, stable manifold; broken line, unstable manifold.

and hence the rate of transport (Camassa & Wiggins 1990). As important as these concepts are from a conceptual viewpoint, they might be, however, of little use in actual flows computed by numerical means. Computing manifolds is contingent upon two factors; the velocity field itself and computer time. In systems of practical interest the velocity field must be obtained numerically and the tracking of manifolds depends on the numerical error in the velocity field itself and the interpolation technique. Naturally the problem does not arise if an analytical expression for the velocity field is available. Figure 6 shows the manifold structure for the closed cavity flow.

The problem considered here, however, is amenable to such an analysis, and moreover, for small perturbations from the integrable case, it can be examined by means of the Melnikov technique (this technique is useful if an analytical expression for the unperturbed homoclinic or heteroclinic orbit is available but is somewhat of limited use in cases where the velocity field must be obtained numerically (see Guckenheimer & Holmes 1983; Wiggins 1988). The perturbed dynamical system can be written as

$$\mathrm{d}x/\mathrm{d}t = f_1(x, y) + \epsilon g_1(x, y; t), \tag{6a}$$

$$\mathrm{d}y/\mathrm{d}t = f_2(x, y) + \epsilon g_2(x, y; t), \tag{6b}$$

where ϵ is the perturbation parameter, $f_1 = \partial\psi_0/\partial y$, $f_2 = -\partial\psi_0/\partial x$, $g_1 = \partial\psi_1/\partial y$, and $g_2 = -\partial\psi_1/\partial x$, with $\psi_0(x, y)$ and $\psi_1(x, y; t)$ as the streamfunction for the unperturbed and perturbed flows respectively. In our case ψ_0 corresponds to the streamlines in figure 1*a*, *c*.

The method gives the number of transverse intersections between the stable and unstable manifolds per period as well as the lobe area, valuable information which could otherwise be only gathered by examination of numerous specific computations. For example, in the case corresponding to figure 1*a* and wall motions given by equation (5), the Melnikov function has zeros at $\frac{1}{2}T$ and T; this means that the stable and unstable manifolds have two transverse intersections per period. For $0.31 < w < \infty$ there is only one (central) heteroclinic orbit; for $0.162 < w < 0.31$ two sets are possible: one separating the two central cells, the others between the wall cells and the central cells (see figure 1*c*). We focus on the central heteroclinic orbit. Let us define the wall displacement per period as

$$D = (|d_{\mathrm{top}}| + |d_{\mathrm{bot}}|)/w, \tag{7}$$

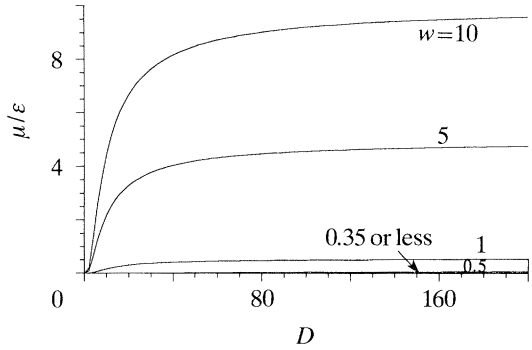

Figure 7. Effect of wall displacement and aspect ratio on lobe area from Melnikov analysis for the driven cavity flow; $r = 1.0$.

Table 3. *Eulerian and lagrangian descriptions of transport*

	eulerian	lagrangian
governing equation	$\partial\theta/\partial t + \boldsymbol{u}\cdot\nabla\theta = \kappa\nabla^2\theta$	$\mathrm{d}\boldsymbol{x}/\mathrm{d}t = \boldsymbol{u}(\boldsymbol{x},t) + \boldsymbol{\zeta}(t)$
typical cases	heating of a fluid; dissolution of a solute wall into a liquid	dispersion of a blob of dye; dispersion of a hot spot
typical initial conditions	$\theta(\boldsymbol{x},0) = \theta_0$	$\theta(\boldsymbol{x},0) = \theta_0\,\delta(\boldsymbol{x}-\boldsymbol{x}_0)$
typical boundary conditions	$\theta(\partial\boldsymbol{\Omega},t) = \theta_1$	$\partial\theta/\partial n = 0$ on $\partial\boldsymbol{\Omega}$

with
$$d_{\mathrm{top}} = \int_0^T u_{\mathrm{top}}(t)\,\mathrm{d}t; \quad d_{\mathrm{bot}} = \int_0^T u_{\mathrm{bot}}(t)\,\mathrm{d}t. \tag{8}$$

Figure 7 shows the lobe area (μ) as a function of D for various aspects ratios w. In all cases the lobe area corresponds to the central heteroclinic orbits. For each w the lobe area increases gradually with D and reaches an asymptotic value, at which case only one lobe is possible between the parabolic points. Most of the improvement occurs for $5 < D < 10$. Also for a given D the lobe area increases with aspect ratio and cavities with aspect ratio less than 0.3 are difficult to clean (the lobe area is negligibly small; incidentally, so is the lobe area between the heteroclinic orbits separating the central cells and the wall cells).

The question now is how this underlying chaos affects the transport of diffusing scalars in the flow. Obviously, the extent to which the transport is affected will depend on the ratio between the rate and extent of chaotic advection and speed of molecular diffusion. As we shall show even relatively confined regions of chaos improve transport considerably.

5. Diffusing scalars in chaotic flows

As an example consider the heating of a fluid in a square closed cavity using square wave-form for the wall motions; such a problem is well suited for an eulerian description of transport (see table 3). The energy balance equation is given by:

$$\partial\theta/\partial t + \boldsymbol{u}\cdot\nabla\theta = (1/Pe)\,\nabla^2\theta, \tag{9}$$

where θ is the dimensionless temperature and Pe is the Péclet number, UL/κ, where U is a characteristic velocity, L is a characteristic length, and κ is the thermal

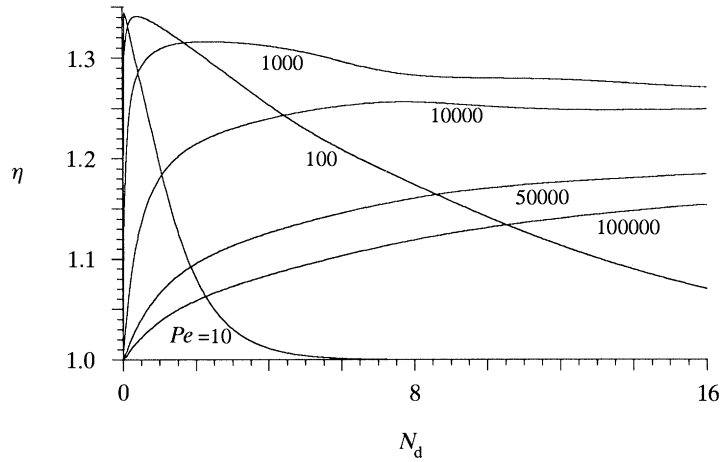

Figure 8. Effect of chaotic flows on diffusing tracers. Heating of a newtonian fluid in a closed cavity. $w = 1.0$, $D = 0.1$ and $r = 1.0$. A square wave-form is used for wall motions.

diffusivity of the fluid. Initially the fluid is at θ_0 and at $t > 0$, a constant temperature of θ_1 is maintained at the surrounding walls. Because of the regular geometry of the cavity and compatible initial and boundary conditions we solve the problem using a finite-difference technique. To quantify the effect of chaotic advection it is convenient to define two additional parameters. The total wall displacement, N_d, is defined as the product of D and the total number of periods (P); i.e. $N_d = DP$. The enhancement factor η, is defined as the ratio of the average temperature of the fluid using the chaotic flow to that produced by the application of the regular flow for the same value of N_d (N_d is a measure of the cost incurred in moving the walls). Figure 8 shows the variation of η as function of N_d for different values of Pe. It is apparent that there is an interplay between thermal diffusion and chaotic advection and that substantial improvements are possible (it should be noted that the amount of chaos in this flow is mostly confined to narrow bands near the heteroclinic orbit). At low Péclet numbers the thermal diffusion dominates and chaos plays almost no role. At large Péclet numbers a thin thermal boundary layer is formed at the walls; however, this is precisely the region where the flow is typically less chaotic and the effect of chaotic advection is reduced to shuffling portions of materials in the centre region where the temperature is already uniform. The best results are obtained at intermediate Péclet numbers; the temperature gradient is spread over a wider region and the shuffling action of the chaotic advection, taking parcels of hot fluid from the wall region and replacing it by cold centre-region fluid, enhances the rate of heating considerably.

The second example, discussed only cursorily, corresponds to the case of dispersion of a mass of a diffusing tracer initially trapped in an open cavity with $w = 0.6$. The goal is to measure the fraction of the initial mass removed by the flow. These types of problems are ideally suited for a lagrangian description of transport. The starting point is the advection equation

$$\mathrm{d}\boldsymbol{x}/\mathrm{d}t = \boldsymbol{u}(\boldsymbol{x}, t) + \boldsymbol{\zeta}(t), \tag{10}$$

where $\boldsymbol{\zeta}(t)$, which mimics molecular diffusion, has the properties

$$\langle \zeta_i \rangle = 0, \quad \langle \zeta_i(t)\, \zeta_j(t_0) \rangle = 2D_{\mathrm{mol}}\, \delta_{ij}\, \delta(t - t_0) \tag{11}$$

(the pointed brackets $\langle \cdot \rangle$ denote an ensemble average, the subscripts i and j represent ith and jth components respectively, and D_{mol} is the molecular diffusion coefficient). A related study by Shariff *et al.* (1992) for the time-periodic shedding of vortices behind a circular cylinder studied the effect of chaotic advection without considering molecular diffusion.

The initial condition is represented in terms of a collection of particles. The fact that no particles can penetrate the solid walls defines the boundary conditions. The displacements of particles by molecular diffusion is mimicked by generating random numbers with zero mean and standard deviation in the ith direction given by $z_i^2 = 2D_{\mathrm{mol}}\tau$, where τ is the time between two consecutive kicks, called the 'kick time'. The variance z_i has the dimension of length and is a measure of an average displacement in one kick. A value is assigned to z_i and τ is determined from the relation given above. Each particle is advected for a time τ using the flow followed by the brownian displacement to a new location. This is repeated for the entire period of the flow and at the end the fraction of particles removed from the prescribed domain is calculated.

Typical results indicate that the particles are removed in two stages. Most of the particles above the dividing KAM surface are removed within a few periods; the rest is removed by a combination of molecular diffusion and leakage through holes in the perforated KAM surface (so called cantorus, Khakhar *et al.* 1986). The circulation in the cells near the bottom of the cavity is a factor of 10^{-3} less than that of the top part. For this reason, it is advisable to apply the jets in two stages: first, with a low period to remove particles in the upper portion of the cavity, then for a higher period to remove the particles confined to the bottom cell. High-period jets serve two aims; they produce perforations in the KAM surface and induce widespread chaos in the bottom of the cavity. Within a given region advection and diffusion act in parallel; the escape of particles from chaotic regions is controlled by advection through holes; the removal of the particles confined to regions of regularity is governed by molecular diffusion.

6. Outlook

We have introduced the concept of transport enhancement in cellular flows by means of prototypical flows and indicated a few possibilities for further investigations. Analyses have been restricted to time-periodic forcing but generalization to quasiperiodic modulations seems straightforward (Beige *et al.* 1991). Such an extension might have far reaching implications; in particular it might allow connecting near wall Stokes flows with outside forcing turbulent flows. Experiments are undoubtedly necessary but already developed theory provides useful guidance; closed cavities with $w < 0.3$ are inefficient in transporting material between opposing moving walls because of very weak motions in the interior cells and dividing KAM surfaces; similar reasons preclude open cavities with $w < 0.7$ to be completely cleaned by means of laminar jets. The flows considered are relevant in the context of transport processes involving solid or porous surfaces; various engineering applications may not be far behind (see Howes *et al.* 1991). Jet induced cavity flows and backward step flows might be useful in the analysis of cleaning of surfaces, growth and deposition processes near walls, etc. Wall driven cavity flows can be regarded as small pores connecting two separate flows and thus they might be useful in highlighting the role of flows in enhancement of transport in the neighbourhood of porous walls.

PHILOSOPHICAL TRANSACTIONS OF THE ROYAL SOCIETY A MATHEMATICAL, PHYSICAL & ENGINEERING SCIENCES

Future developments can proceed in several directions. One possibility is to focus on heterogeneous fluids which contain suspended material that can aggregate or agglomerate leading to the formation of fractal-like clusters (Danielson *et al.* 1991). One such example is solids formation and growth processes in thermally stressed fluids. Such a situation is important in understanding the fundamentals of fouling processes (fouling related problems, plant shut-down, power requirements to compensate for oversizing, etc., account for 0.3% of the gross national product of the U.S.A. and U.K. (J. M. McMichael, personal communication). Studies might then focus on ways to improve the rate of transport while at the same time to minimize the rate of aggregation. This is essentially an optimization problem; chaos accelerates the rate of aggregation but on the other hand material spends less time in the recirculating regions. Finally, other mechanisms for transport enhancement should be explored as well. The heating example in §5 shows clearly that even small amounts of chaos enhance transport considerably but that chaos does not easily reach to the bottom deep of the cavity (figure 5*b*). Inertia may improve transport in deep cavities and this point should be explored more fully; temperature gradients might help as well. In some instances, such as cleaning, the temperature gradients might be induced by means of exothermic chemical reactions. A knowledge of transport enhancement might allow engineers to look at old processes with new eyes and suggest avenues for process optimization and invention.

We extend our appreciation to C.-W. Leong for providing figure 1*b*, *d* and to P. Moin for allowing us to use the finite-difference code for the flow down a backward step. This work was supported by a grant from the AFOSR.

References

Aref, H. 1984 Stirring by chaotic advection. *J. Fluid Mech.* **143**, 1–21.

Armaly, B. F., Durst, F., Pereira, J. C. F. & Schönung, B. 1983 Experimental and theoretical investigation of backward-facing step flow. *J. Fluid Mech.* **127**, 473–496.

Beige, D., Leonard, A. & Wiggins, S. 1991 Chaotic transport in the homoclinic and heteroclinic tangle regions of quasiperiodically forced two-dimensional dynamical systems. *Nonlinearity* **4**, 775–819.

Broomhead, D. S. & Ryrie, S. C. 1988 Particle paths in wavy vortices. *Nonlinearity* **1**, 409–434.

Burggraf, O. R. 1966 Analytical and numerical studies of the structure of steady separated flows. *J. Fluid Mech.* **24**, 113–151.

Camassa, R. & Wiggins, S. 1990 Chaotic advection in a Rayleigh–Bénard flow. *Phys. Rev.* A **43**, 774–797.

Chaiken, J., Chevray, R., Tabor, M. & Tan, Q. M. 1986 Experimental study of lagrangian turbulence in a Stokes flow. *Proc. R. Soc. Lond.* A **408**, 165–174.

Chebbi, B. & Tavoularis, S. 1990 Low Reynolds number flow in and above asymmetric, triangular cavities. *Phys. Fluids* A **2**, 1044–1046.

Chien, W. L., Rising, H. & Ottino, J. M. 1986 Laminar mixing and chaotic mixing in several cavity flows. *J. Fluid Mech.* **170**, 355–377.

Chilukuri, R. & Middleman, S. 1983 Circulation, diffusion, and reaction within a liquid trapped in a cavity. *Chem. Engng Commun.* **22**, 127–138.

Chilukuri, R. & Middleman, S. 1984 Cleaning of a rough rigid surface: removal of a dissolved contaminant by convection-enhanced diffusion and chemical reaction. *J. electrochem. Soc.* **131**, 1169–1173.

Danielson, T. J., Muzzio, F. J. & Ottino, J. M. 1991 Aggregation and structure formation in chaotic and regular flows. *Phys. Rev. Lett.* **66**, 3128–3131.

Davey, A., DiPrima, R. C. & Stuart, J. T. 1968 On the instability of the Taylor vortices. *J. Fluid Mech.* **31**, 17–52.

PHILOSOPHICAL TRANSACTIONS OF THE ROYAL SOCIETY A MATHEMATICAL, PHYSICAL & ENGINEERING SCIENCES

Goodrich, J. & Soh, W. Y. 1989 Time-dependent viscous incompressible Navier–Stokes equations: the finite difference Galerkin formulation and streamfunction algorithms. *J. Comput. Phys.* **84**, 207–241.

Guckenheimer, J. & Holmes, P. 1983 *Nonlinear oscillations, dynamical systems, and bifurcations of vector field*. New York: Springer-Verlag.

Higdon, J. J. L. 1985 Stokes flow in arbitrary two-dimensional domains: shear flow over ridges and cavities. *J. Fluid Mech.* **159**, 195–226.

Higdon, J. J. L. 1990 Effect of pressure gradients on Stokes flows over cavities. *Phys. Fluids* A **2**, 112–114.

Howes, T., Mackley, M. R. & Roberts, E. P. L. 1991 The simulation of chaotic mixing and dispersion for periodic flows in baffled channels. *Chem. Engng Sci.* **46**, 1669–1677.

Jeffrey, D. J. & Sherwood, J. D. 1980 Streamline patterns and eddies in low-Reynolds-number flow. *J. Fluid Mech.* **96**, 315–334.

Khakhar, D. V., Rising, H. & Ottino, J. M. 1986 Analysis of chaotic mixing in two model flows. *J. Fluid Mech.* **172**, 419–451.

Kim, J. & Moin, P. 1985 Application of fractional step method to incompressible Navier-Stokes equations. *J. Comput. Phys.* **59**, 308–323.

Küblebeck, K., Merker, G. P. & Straub, J. 1980 Advanced numerical computation of two-dimensional time-dependent free convection in cavities. *Int. J. Heat Mass Transfer* **23**, 203–217.

Leong, C.-W. 1990 Chaotic mixing of viscous fluids in time-periodic cavity flows. Ph.D. dissertation, University of Massachusetts, U.S.A.

Leong, C.-W. & Ottino, J. M. 1989 Experiments on mixing due to chaotic advection in a cavity. *J. Fluid Mech.* **209**, 463–499.

Moffatt, H. K. 1964 Viscous and resistive eddies near a sharp corner. *J. Fluid Mech.* **18**, 1–18.

Mullin, T., Cliffe, K. A. & Pfister, G. 1987 Unusual time-dependent phenomena in Taylor–Couette flow at moderately low Reynolds number. *Phys. Rev. Lett.* **58**, 2212–2215.

O'Brien, V. 1975 Unsteady separation phenomena in a two-dimensional cavity. *AIAA J.* **13**, 415–416.

Ottino, J. M. 1989 *The kinematics of mixing: stretching, chaos, and transport*. Cambridge University Press.

Pan, F. & Acrivos, A. 1967 Steady flows in rectangular cavities. *J. Fluid Mech.* **28**, 643–655.

Rom-Kedar, V. & Wiggins, S. 1990 Transport in two-dimensional maps. *Arch. ration. Mech. Analysis* **109**, 239–298.

Ryu, H. W., Chang, H. N. & Lee, D. I. 1986 Creeping flows in rectangular cavities with translating top and bottom walls: numerical study and flow visualization. *Korean J. chem. Engng* **3**, 177–185.

Shariff, K., Pulliam, T. H. & Ottino, J. M. 1992 A dynamical systems analysis of kinematics in the time-periodic wake of a circular cylinder. In *Vortex dynamics and vortex methods* (ed. C. Anderson & C. Greengard), *Proc. AMS-SIAM Conf.*, Lectures in Applied Mathematics. Providence: American Mathematical Society. (In the press.)

Solomon, T. H. & Gollub, J. P. 1988 Chaotic particle transport in time-dependent Rayleigh–Bénard convection. *Phys. Rev.* A **38**, 6280–6286.

Swanson, P. D. 1991 Regular and chaotic mixing of viscous fluids in eccentric rotating cylinders. Ph.D. dissertation, University of Massachusetts, U.S.A.

Swanson, P. D. & Ottino, J. M. 1990 A comparative computational and experimental study of chaotic mixing of viscous fluids. *J. Fluid Mech.* **213**, 227–249.

Tighe, S. & Middleman, S. 1985 An experimental study of convection-aided removal of a contaminant from a cavity in a surface. *Chem. Engng Commun.* **33**, 149–157.

Weiss, R. F. & Florsheim, B. H. 1965 Flow in a cavity at low Reynolds number. *Phys. Fluids* **8**, 1631–1635.

Wiggins, S. 1988 *Global bifurcations and chaos*. New York: Springer-Verlag.

PHILOSOPHICAL TRANSACTIONS OF THE ROYAL SOCIETY A MATHEMATICAL, PHYSICAL & ENGINEERING SCIENCES

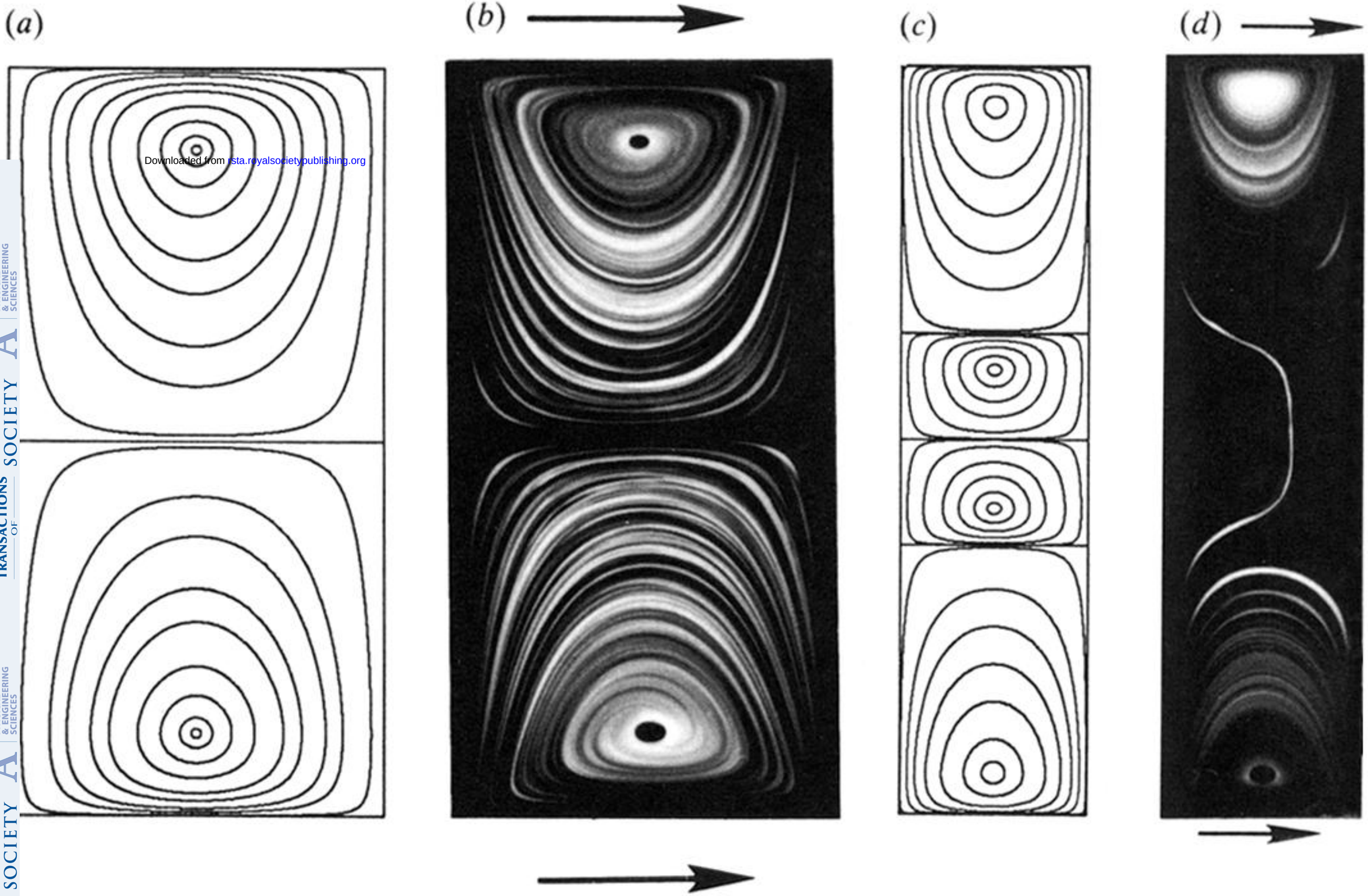

Figure 1. Steady streamline portraits for flow in a driven rectangular cavity. (*a*) Computation with $r = 1$ and $w = 0.5$. (*b*) Experiment with $r = 1$ and $w = 0.5$. (*c*) Computation with $r = 1$ and $w = 0.25$. (*d*) Experiment with $r = 1$ and $w = 0.25$. Both the top and bottom walls move from left to right.